npg

ORIGINAL ARTICLE

Analysis of the end-segment distribution of a polymer at the interface of filler-filled material

Hiroshi Morita[1], Masatoshi Toda[1] and Takashi Honda[2]

The distribution of ends of polymers in a filler-filled material is simulated using self-consistent field method. In our simulation results, segregation of the ends of a polymer can be found at the interface of filler, although the depletion region of the ends also exists within a distance of gyration radius (Rg) from the filler. The sizes and shapes of the filler are affected by the segregation of the ends of a polymer. In the case of small or spherical fillers, the density of the ends of the polymer near the interface of filler increases. These results can be explained by the entropic effect of polymer chain ends. The segregation of ends contributes to the stabilization at the interface of the filler, thus adding the entropic part of the free energy.

INTRODUCTION

Filler-filled materials are now considered to be fundamental materials, and many researchers have studied their processing and functions. The physical properties and the functions of composite materials are closely related to those of the dispersed structures of fillers, and the dispersion of the filler must be controlled in the fabrication process.[1,2] For this reason, many researchers have studied the techniques for the dispersion of fillers. The research areas addressing those techniques are extensive. For example, from the point of view of a material, to make the interaction between polymer and filler an attractive one, the surface of the filler or the polymer are chemically modified in some cases.[3]

A typical example of a filler-dispersed material is the rubber material used for tires. In highly functional rubber for tire, the end-functional (or modified) polymer is used to control the dispersion of silica or carbon black fillers in rubbers.[4] In these polymers, the end groups of polymer are modified to the attractively interacted substituent group to filler, and it is believed that the ends of the polymers will be trapped at the interface of fillers. It is also known that this modification of polymer ends affects the loss energy, and this situation contributes to the fuel efficiency of automobiles. Therefore, the design and the control of the ends of polymers are very important for the development of composite materials.

Analysis of the distribution of end groups is important within regions of confined geometry, and this distribution is commonly studied using simulations. One of the more typical methods for studying the ends of polymer chains is the use of the self-consistent field (SCF) method.[5–7] The details of the SCF method will be described later. In short, the distribution of each segment in a polymer chain can be estimated, and the density profile of the ends in a system can also be obtained. Furthermore, using coarse-grained molecular dynamics simulation[8] or molecular Monte Carlo (MC) simulation,[9] the distribution of the end particles can also be simulated. In the case of an interface between a polymer and a solid plate, the segregation of polymer chain ends can be estimated using MC[10–12] and MD[13] simulations. In the case of the surface of a polymer thin film, by using SCF and coarse-grained molecular dynamics simulations, the end-segment segregation and its dynamics at the surface can be simulated.[14] The results of this analysis have already been obtained by some experiments.

The statistics and the dynamics of each part in a polymer chain are not uniform. From the point of view of a single polymer chain, the generation and annihilation of entanglement occur owing to the fluctuating motion of the polymer ends.[15] Because the end parts of a polymer can adopt many conformations, those parts become the high entropy parts of polymer chains. At the surface of a polymer thin film, the segregation of the end parts of a polymer occurs owing to stabilization by the entropic effect.[14] Similarly, the end parts are also segregated at the interface between a polymer and a substrate.[16] Therefore, inhomogeneous distribution of the polymer ends is expected in a filler-filled polymer system.

In this study, the end-segment distribution of a polymer in a filler-filled material is studied using an SCF simulation. In Model and Simulation, details of the modeling of the filler-filled system on the basis of coarse-graining techniques with the SCF theory are described. In Results and Discussions, the simulation results are discussed. The end-segment distribution near both fiber-type and spherical fillers is calculated, and the dependences of the interactions between end segments and a filler (e.g., molecular weight of the polymer and particle size of the filler) are examined.

[1]Research Center for Computational Design of Advanced Functional Materials, National Institute of Advanced Industrial Science and Technology (AIST), Ibaraki, Japan and [2]Zeon Corporation, Kanagawa, Japan
Correspondence: Dr H Morita, Research Center for Computational Design of Advanced Functional Materials, National Institute of Advanced Industrial Science and Technology (AIST), Central 2-1, 1-1-1 Umezono, Tsukuba, Ibaraki, 305-8568, Japan.
E-mail: h.morita@aist.go.jp

MODEL AND SIMULATION

Self-consistent field method

Equations for the SCF method were solved using the ordinal technique.[5–7]

In this study, to minimize the free energy of the system, the segment density distributions $\phi(\mathbf{r},s)$ are adjusted with changing potential field and path integrals, where $\mathbf{r}$ is the mesh position and s is the index of the segment along a polymer chain. The statistical weight of the chain conformation in a potential field $V(\mathbf{r})$, the path integral $Q^{\pm}(\mathbf{r},s)$, is calculated by the following equation

$$\frac{\partial}{\partial s}Q^{+}(\mathbf{r},s) = \left[\frac{b^2}{6}\nabla^2 + V(\mathbf{r})\right]Q^{+}(\mathbf{r},s), \text{(from } s=0 \text{ to } s=N)$$

(1a)

$$\frac{\partial}{\partial s}Q^{-}(\mathbf{r},s) = \left[\frac{b^2}{6}\nabla^2 + V(\mathbf{r})\right]Q^{-}(\mathbf{r},s), \text{(from } s=N \text{ to } s=0)$$

(1b)

with the initial condition

$$Q^{+}(\mathbf{r},0) = 1, Q^{-}(\mathbf{r},0) = 1,$$

(2a)

where b is the Kuhn segment size, and N is the length of the polymer chain. The signs $+$ and $-$ specify the directions of the calculation where the $+$ sign indicates the forward direction (Equation (1a)), and the $-$ sign indicates the backward (Equation (1b)) direction along the chain.
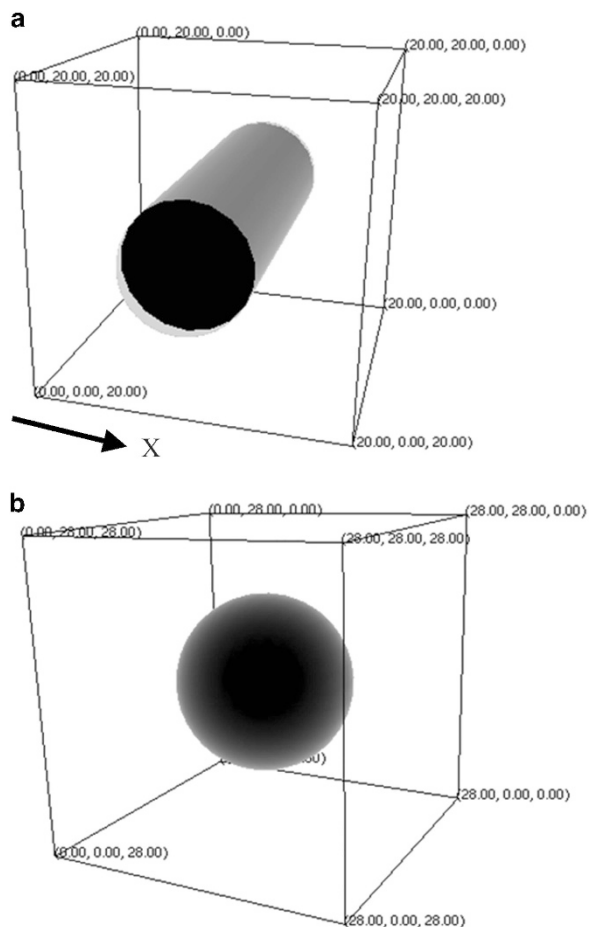
a

b

Figure 1 Model structures of the fillers. (**a**, **b**) The models for fiber-type and spherical fillers, respectively.

At a wall boundary, the following initial condition is used,

$$Q^{+}(\mathbf{r}',0) = 1/y(\mathbf{r}'), Q^{-}(\mathbf{r},0) = 1/y(\mathbf{r}'),$$

(2b)

where $y(\mathbf{r}')$ is the Jacobian for the filler at the mesh point. To calculate $y(\mathbf{r}')$, one mesh point is divided into sub-mesh points, and the number of interfacial points of the filler is counted. The fraction of interfacial points within the sub-mesh space is applied to $y(\mathbf{r}')$.

In Equations 1a and 1b, the segment density $\phi(\mathbf{r},s)$ is obtained using the path integral as

$$\phi(\mathbf{r},s) = n\frac{\int ds\, Q^{+}(\mathbf{r},s)\, Q^{-}(\mathbf{r},N-s)}{\int d\mathbf{r}\int ds\, Q^{+}(\mathbf{r},s)\, Q^{-}(\mathbf{r},N-s)},$$

(3)

where n is the total number of chains in the system. Equations (1) and (3) are mutually coupled through the following definition of $V(\mathbf{r})$,

$$V(\mathbf{r}) = \chi\phi(\mathbf{r}) + \gamma(\mathbf{r}),$$

(4)

where χ is the Flory–Huggins interaction parameter, and $\gamma(\mathbf{r})$ is the Lagrange multiplier for the local incompressible condition,

$$\sum_{s}\phi(\mathbf{r},s) = \text{constant.}$$

(5)

When Equations (1a)–(5) are solved self consistently, the set of the SCF V, the density ϕ, and the path integral Q can be obtained, and the segment densities of $\phi(\mathbf{r},s)$ are also calculated. Convergence is checked using the criteria for the SCF V, the density ϕ, and the total free energy. The threshold value is 1.0×10^{-5}. All of the SCF simulations were conducted using SUSHI simulator (version 10.0, 2015.03.10) in OCTA system.[17]

Model of the filler

In the simulations of filler-filled material, the filler must be modeled on the basis of the coarse-grained technique of SCF method. In the SCF simulation, because the polymer is described as the density profile on each mesh, the filler is modeled as filler-shaped mesh points where all polymers are excluded. The density of the polymer at the mesh point inside the filler becomes zero. Furthermore, the interfacial interaction must be included to represent the interaction between the polymer and the filler under the condition that the surface of the filler is not always on the mesh points.

In the SCF simulation using the SUSHI simulator of OCTA, the function of 'obstacle' can be used to represent the filler. Using the SUSHI simulator, to include a short-range interaction between the polymer and the filler, the surface χ parameter of the filler (χ_{FP}) is introduced. At each mesh point near $\mathbf{r}$ from the filler interface, SCF $V(\mathbf{r})$ is calculated using the following equation instead of Equation (4),

$$V(\mathbf{r}) = \chi\phi(\mathbf{r}) + \chi_{FP}\phi(\mathbf{r}')y(\mathbf{r}') + \gamma(\mathbf{r}),$$

(6)

where $\mathbf{r}'$ is the mesh position at the nearest neighbor from the filler interface, and $y(\mathbf{r}')$ is the Jacobian for the filler at the mesh point written in Equation (2b). In this study, the width of the sub-mesh points is set to $b/100$.

Simulation conditions

The SCF simulations were performed using a three-dimensional mesh system with a three-dimensional shape for the filler. In the case of a fiber-type filler, the radius R of a fiber is $4.0b$ or $8.0b$, and the length of a fiber is $20b$. The filler is placed at the center of the simulation box, and the axial direction of the filler is set to the z direction. The distances between the surface of a fiber and the boundary in the x and

y directions are set to 6.0b and in the z direction is set to 0.0. Therefore, in the cases of the fibers of $R=4.0b$ and $R=8.0b$, the system sizes become $20\times20\times20$ and $28\times28\times20$, respectively. Because all mesh widths are set to 0.5 on the regular mesh system, the total mesh sizes for $R=4.0b$ and $R=8.0b$ are $40\times40\times40$ and $56\times56\times40$, respectively. Periodic boundary conditions are used in all directions.

In the simulated system, only the polymer and a single filler are included. The structures for the cases of fiber type and spherical fillers are shown in Figures 1a and b, respectively. The χ parameter between the polymers is set to 0.0. Polymers with lengths of $N=100$, 200 and 500 were studied. In the SCF simulation, N is the same as the total number of segments that have a size of b, and $\phi(\mathbf{r},0)$ is defined as the end-segment density at mesh position $\mathbf{r}$. Where polymers interacted with fillers, χ_{FP} was set to 0.0. Thus, interactions between polymers and between the polymer and filler were the same. Furthermore, to calculate the end-functional polymer, χ_{FP} for the end χ_{FPE} was introduced, and χ_{FPE} was set to 0.0, -0.05, -0.1.

RESULTS AND DISCUSSIONS

Figure 2 shows the density profile of the polymer along the axis across the center of a fiber. This simulation result is obtained using simulation conditions of $\chi=0.0$, $\chi_{FP}=0.0$ and $N=100$. In Figure 2, the density profiles of both one-sided end and middle 98 segments are plotted. Because periodic boundary conditions were applied in this simulation, the position of $x=20.0$ is equivalent to the position $x=0.0$. At $x=0.0$ and 20.0, the end-segment density becomes ~0.01. This value is the same as the bulk value for end segments. At $x=0.0$ and 20.0, bulk structure unperturbed by filler is represented, even though the system size of 20.0 is not large. Therefore, this simulation will produce a qualitatively correct result.

In Figure 2, at the central part along the horizontal axis, the density of the polymer is zero, and this region is occupied by the filler. At both the left and right sides of the filler, the density of the end segments increases. This result indicates that end-segment segregation occurs at the interface of the filler. On the other hand, around $x=5.0$ and 15.0, a depletion of the end segments can be found. Therefore, it can be
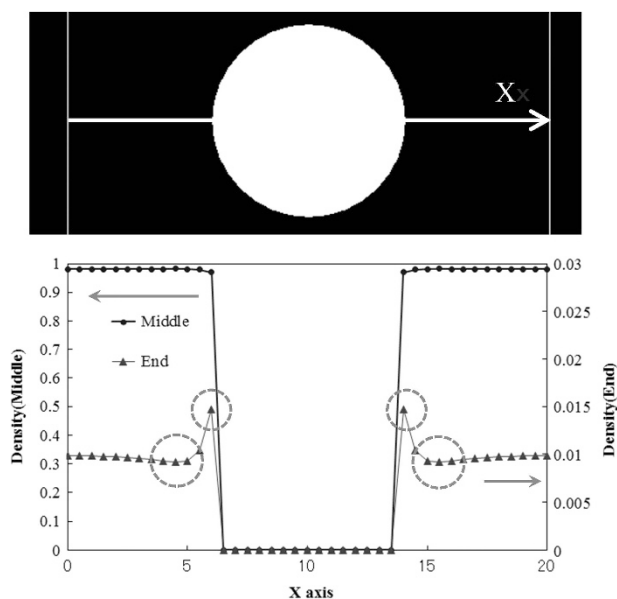
found that many end segments of polymers within the distance of Rg from filler are shifted to the fillers.

This result can be explained with consideration for the free energy. Free energy comprises distinct entropy and enthalpy parts, and these two parts are always balanced to stabilize the system. At the interface between a solid flat wall and a polymer, if the end parts with a high entropic energy are segregated at the interface, as shown in Figure 3 (1), this interface becomes stabilized by the entropic effect of the polymer. On the other hand, if a polymer has an attractive interaction with a solid wall as shown in Figure 3 (2), the polymer adopts a tail-loop-train conformation,[7,18] and this interface becomes stabilized by the enthalpy effect of attractive interactions between the polymer segment and the wall. In the SCF simulation presented here, an attractive interaction owing to the χ parameter between the polymer and the filler is not imposed. Therefore, the origin of the segregation of the end parts can be explained by the entropic effect. The SCF simulation results are mapped to the cartoon shown in Figure 3 (3), in which segregation and depletion of the end parts near the filler are presented.
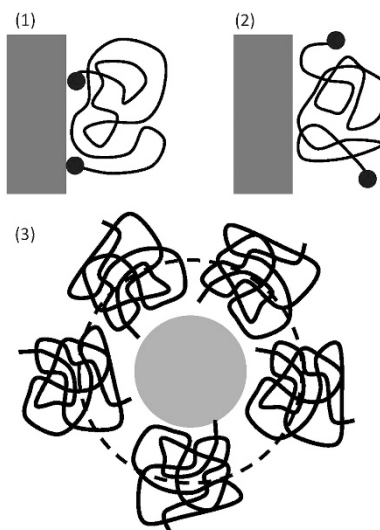

Figure 3 Typical chain conformations driven by (1) enthalpy and (2) entropy energies, and (3) a cartoon representing the conformation of a polymer chain near a filler.
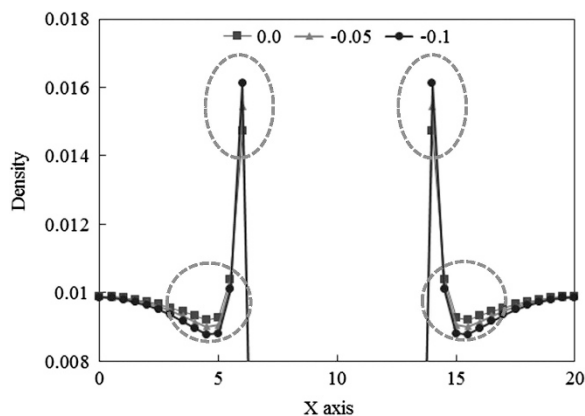

Figure 2 Density profiles of middle and end segments along the x axis.

Figure 4 End segment distributions with different χ_{FPE} parameters (χ_{FPE} is the χ parameter between the end of the polymer and the filler).
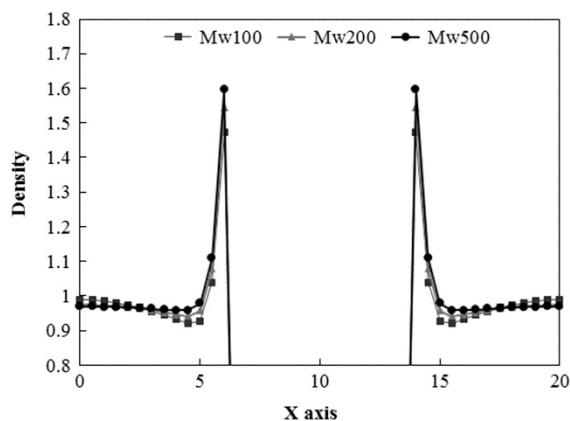
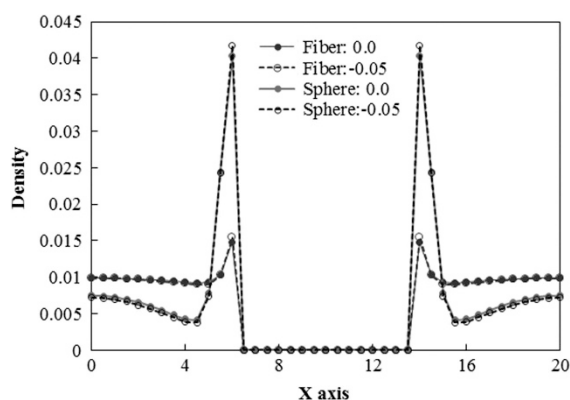Figure 5 End segment distributions with different molecular lengths of the polymer.

Figure 6 Comparison between end-segment distributions for spherical and fiber-type fillers.
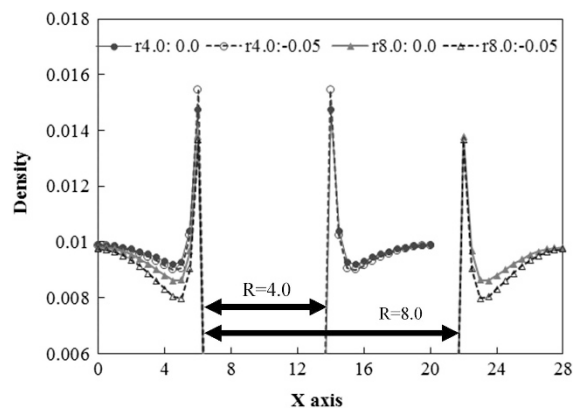

Figure 7 Comparison between end-segment distributions for the radius of filler values of $R = 4.0$ and $R = 8.0$.
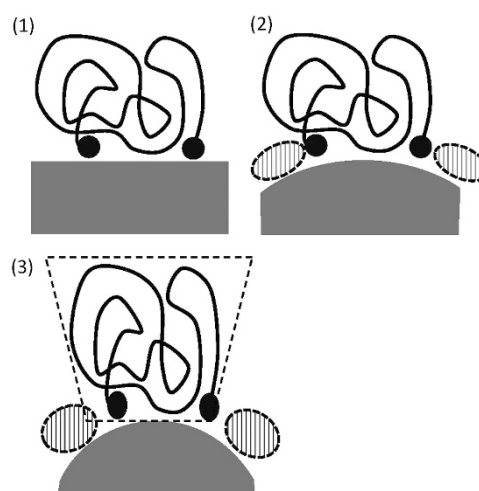

Figure 8 A cartoon to aid in explaining the effects of the curvature of fillers on the conformation of interacting polymer chains. (1), (2), and (3) show the polymer chain attached to flat, curved and more curved surfaces, respectively.

Next, simulations for the polymer ends were performed, and the effect of attractive interaction between end segments and the filler was examined. Because the interaction between the polymer and the filler is described by χ_{FP}, χ_{FP} for the end segment χ_{FPE} was introduced. As the χ parameter becomes smaller, the targeted materials can be mixed, and they interact in an attractive manner. Figure 4 shows the end-segment distribution of the filler using $\chi_{FPE} = 0.0$, -0.05, and -0.1. As χ_{FPE} becomes smaller, the density of the end segment at the interface of the filler increases, and the depletion of density is enhanced. From these simulation results, it is evident that the functional ends of the polymer effectively segregate at the interface of filler.

It is important to note the effect of molecular weight on the segregation of polymer end segments at the interface of filler. If the molecular weight increases, the fraction of end segments decreases and the total number of end segments per unit also decreases. This affects the balance of free energy between entropy and enthalpy, and the amount of segregation of end segments at the interface is changed. Figure 5 shows the end-segment distribution at the interface for various polymer lengths. Here the lengths of polymers of 100, 200 and 500 are calculated. As described before, if the length of a polymer is changed, the fraction of the end segments is also changed. For this reason, the density of end segments shown in the vertical axis of Figure 5 is normalized by the bulk density of end segments. On the basis of the simulation results, as the length of the polymer increases, the end-segment density at the interface increases. Note that the end-segment density at $x = 0.0$ and 20.0 is not equal to 1.0, especially

in the case of $N = 500$. This indicates that at $x = 0.0$ and 20.0, the end-segment density does not converge to the bulk value. This result can be derived from the effect of the system size. If the length of a polymer increases, then the Rg of that polymer also increases. In this calculation, the distance from the filler interface to the boundary, which is fixed at 6.0, is not sufficient to converge the end-segment density at the boundary for the case of $N = 500$. Therefore, the result of $N = 500$ must be taken into the boundary effect carefully.

The SCF simulation of a spherical filler system was also performed. In the case of a fiber-type filler, the local shape in the radial direction is curved, but the shape in the axial direction is flat. In contrast, the surface of a spherical filler has a curvature everywhere. This is the primary difference between spherical and fiber-type fillers. Figure 6 shows the end-segment densities in the systems of both spherical and fiber-type fillers. In the case of a spherical filler, the density profile along the x axis across the center of a sphere is plotted. At the interface of filler, the end-segment densities of spherical and fiber-type fillers are approximately 0.015 and 0.04, respectively, and the density of a spherical filler is ~ 2.5 times larger than that of a fiber-type filler. An explanation for these results is closely related to the curvature of

the filler. This is discussed later, combined with the results for changing the radius of the filler shown in Figure 7.

If the radius R of a fiber is changed, then the curvature at the interface of the filler changes along $1/R$, and the conformation of the polymer chain is impacted. To examine the effect of the radius of the fiber, simulations using radii of $R = 4.0$ and 8.0 were performed. Figure 7 shows the results of the end-segment distribution for $R = 4.0$ and 8.0. The end-segment density at the interface in the case of $R = 4.0$ is ~ 0.15, and that in the case of $R = 8.0$ is ~ 0.135. The end-segment density of the thin fiber is ~ 1.1 times larger than that of the thick fiber.

The effects due to the radius of the fiber and the structure of the filler are explained by the curvature of the interface of filler. At the interface, the polymers are attached to the filler. Although it is well known that a single polymer chain adopts a string-like conformation, its conformation is deformed at the interface of fillers. In addition, the position of the end segments are adjusted to stabilize the free energy. As shown in Figure 3, to stabilize the free energy, the segregation of the end segment at the interface of filler contributes to minimizing the free energy at the interface. It is expected that this stabilization is changed in the case of a curved interface of filler. In Figure 8, cartoons illustrating flat and curved interfaces are shown. In the case of the flat interface shown in Figure 8 (1), the stabilization is maintained by both the enthalpy effect derived from the interaction of the middle region of the polymer and the entropy effect by the segregation of end segments at the interface. In contrast, for the curved interface shown in Figure 8 (2), the contact area is limited, and it is brought out of the empty space shown by the shaded area before the deformation of the polymer. If the string-like spherical shape of a polymer chain approaches the curved filler, then it is difficult to fill the shaded area with the spherical-shaped polymer. To fill that area, the polymer chain must be deformed. Therefore, the end segments are gathered in the interfacial region, and the interface is stabilized mainly by the entropy effect.

Along this discussion, the difference of filler type and that of radius of fillers can be explained. In the case of spherical and fiber-type fillers, a spherical filler has a large curvature, and all the surface area of filler has the same curvature. On the other hand, in the case of fiber-type filler, the interfacial structure along the axial direction is flat, but the interface along the radial direction has a curvature. Therefore, the effect due to curvature becomes smaller for the fiber-type filler, and the segregation of end segments becomes less than that of a spherical filler. As the radius of a filler decreases, the curvature at the surface of the filler increases, and the shaded region shown in Figure 8 (3) becomes larger. To fill this region, more end segments will be moved to this region. Note that a radius of filler smaller than the Rg of the polymer is not discussed here. If the radius becomes much smaller than Rg, then the filler will migrate into the space between the polymer chains, disrupting the stabilization mechanism and changing the results.

CONCLUSIONS

In this paper, the end-segment distribution of a polymer near a filler is discussed with results from SCF simulations. End segments can be segregated around a filler, and those results can be found using SCF simulations under conditions in which the interaction between the filler and the polymer is the same as that between polymers. The functionalized end of a polymer affects the segregation of the end at the interface of filler. The segregation of end segments can be explained using the entropy effect. The trends of the segregation of end segments with changes to the radius of the filler and the shape of the filler are explained by the entropy effect due to the curvature of the filler. Because this simulation method is the general simulation method used to study the distribution of polymers in a filler-filled system, this method can also be applied to other filler-filled systems, such as plate-type fillers, rectangular hexahedrons and so on. Further SCF simulations will derive interesting results for the distribution of end segments in a filler-filled system. Furthermore, this method can be used to study the density profile of a polymer in an aggregated filler system. In the near future, we will study these systems using this simulation technique, and interesting results concerning the inhomogeneous distribution of polymers in these filler-filled systems will be discussed.

1 Bhowmick A. K. (ed.). *Current Topics in Elastomers Research*, (CRC Press, NewYork, NY, USA, 2008).
2 Vilgis, T. A., Heinrich, G. & Klüppel, M. *Reinforcement of Polymer Nano-Composites* (Cambridge University Press, Cambridge, UK, 2009).
3 Castellano, M., Conzaatti, L., Costa, G., Falqui, L., Turturro, A., Valenti, B. & Negroni, F Surface modification of silica: 1. Thermodynamic aspects and effect on elastomer reinforcement. *Polymer* **46**, 695–703 (2005).
4 Bohm, G. A., Tomaszewski, W., Cole, W. & Hogan, T. Furthering the understanding of the non linear response of filler reinforcement elastomers. *Polymer* **51**, 2057–2068 (2010).
5 Matsen, M. W. & Schick, M. Stable and unstable phases of a diblock copolymer melt. *Phys. Rev. Lett.* **72**, 2660–2663 (1994).
6 Helfand, E. & Wasserman, Z. R. Block copolymer theory 4. Narrow interphase approximation. *Macromolecules* **9**, 879–888 (1976).
7 Fleer, G. J., Cohen Stuart, M. A., Scheutjens, J. M. H. M., Cosgrove, T. & Vincent, B. *Polymers at Interfaces* (Chapman & Hall, London, UK, 1993).
8 Kremer, K. & Grest, G. S. Dynamics of entangled linear polymer melts: A molecular-dynamics simulation. *J. Chem. Phys.* **92**, 5057–5086 (1990).
9 Binder, K. *Monte Carlo and Molecular Dynamics Simulations in Polymer Sciences* (Oxford University Press, UK, 1995).
10 Kumar, S.K., Vacatello, M. & Yoon, D.Y. Off-lattice Monte Carlo simulations of polymer melts confined between two plates. *J. Chem. Phys.* **89**, 5206–5215 (1988).
11 Vacatello, M., Yoon, D.Y. & Laskowski, B. Molecular arrangements and conformations of liquid n-tridecane chains confined between two hard walls. *J. Chem. Phys.* **93**, 779–786 (1990).
12 Kumar, S.K., Vacatello, M. & Yoon, D.Y. Off-lattice Monte Carlo simulations of polymer melts confined between two plates. 2. Effects of aration. *Macromolecules* **23**, 2189–2197 (1990).
13 Bitsanis, I. & Hadziioannou, G. Molecular dynamics simulations of the structure and dynamics of confined polymer melts. *J. Chem. Phys.* **92**, 3827–3847 (1990).
14 Morita, H., Tanaka, K., Kajiyama, T., Nishi, T. & Doi, M. Study of the glass transition temperature of polymer surface by coarse-grained molecular dynamics simulation. *Macromolecules* **39**, 6233–6237 (2006).
15 Doi, M. & Edwards, S. F. *The Theory of Polymer Dynamics* (Oxford Scientific Publications, Oxford, UK, 1986).
16 Tanaka, K., Tateishi, Y., Okada, Y., Nagamura, T., Doi, M & Morita, H. Interfacial Mobility of Polymers on Inorganic Solids. *J. Phys. Chem. B* **113**, 4571–4577 (2009).
17 Doi, M. OCTA (2002), http://octa.jp/. Accessed 4 May 2015.
18 Morita, H, Ikehara, T., Nishi, T. & Doi, M. Study of Nanorheology and Nanotribology by Coarse-grained Molecular Dynamics Simulation. *Polymer J.* **36**, 265–269 (2004).